

¹ Mesoporous Silica Encapsulated Platinum–Tin Intermetallic ² Nanoparticles Catalyze Hydrogenation with an Unprecedented 20% ³ Pairwise Selectivity for Parahydrogen Enhanced Nuclear Magnetic ⁴ Resonance

⁵ Yong Du, Ranjan K. Behera, Raghu V. Maligal-Ganesh, Minda Chen, Tommy Yunpu Zhao,
⁶ Wenyu Huang,* and Clifford R. Bowers*



Cite This: <https://doi.org/10.1021/acs.jpcllett.2c00581>



Read Online

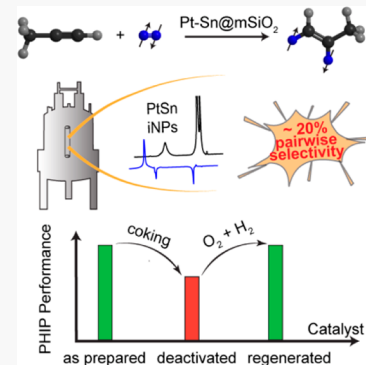
ACCESS |

Metrics & More

Article Recommendations

Supporting Information

ABSTRACT: Supported noble metals offer key advantages over homogeneous catalysts for in vivo applications of parahydrogen-based hyperpolarization. However, their performance is compromised by randomization of parahydrogen spin order resulting from rapid hydrogen adatom diffusion. The diffusion on Pt surfaces can be suppressed by introduction of Sn to form Pt–Sn intermetallic phases. Herein, an unprecedented pairwise selectivity of $19.7 \pm 1.1\%$ in the heterogeneous hydrogenation of propyne using silica encapsulated Pt–Sn intermetallic nanoparticles is reported. This high level of selectivity exceeds that of all supported metal catalysts by at least a factor of 3. Moreover, the pairwise selectivity for alkyne hydrogenation is about 2 times higher than for alkene hydrogenation, an observation attributed to the higher coverage of the former and its effect on diffusion. Lastly, PtSn@*m*SiO₂ nanoparticles exhibited improved coking resistance, and any loss of activity is shown to be fully reversible through high-temperature oxidation–reduction cycling.



Parahydrogen-based hyperpolarization is an efficient and inexpensive method for sensitivity enhanced NMR spectroscopy and imaging.^{1–3} Conversion of the proton singlet spin order of parahydrogen (p-H₂) into NMR observable hyperpolarization is mediated by chemical hydrogenation into magnetically inequivalent sites, resulting in high-field proton NMR signal enhancements that can in theory exceed 4 orders of magnitude. An essential requirement of parahydrogen-based hyperpolarization is pairwise addition, where the pair of H atoms that are incorporated into the hydrogenation adduct originate from the same p-H₂ molecule. Parahydrogen enhanced NMR by heterogeneous catalysis would be highly suitable for in vivo applications, where the hyperpolarized reaction products are readily separable from the insoluble solid catalyst material. However, the maximum reported pairwise selectivity for a monometallic supported nanoparticle catalyst is around 6–7% for hydrogenation of propene over highly dispersed Rh/TiO₂ or atomically dispersed Pt/CeO₂.^{4,5} Incorporating a promoter metal such as Sn to form Pt–Sn bimetallic NPs can improve selectivity for many reactions, including hydrogenations, and can also suppress C–C bond cleavage that leads to carbon deposition and catalyst deactivation.^{7,9} These effects have been ascribed to the lowering of the adsorption energy of the hydrocarbons and have been studied by temperature-programmed desorption (TPD),¹⁰ Auger electron spectroscopy (AES),¹⁰ low-energy electron diffraction (LEED),^{6,7,10–15} and density functional

theory (DFT).^{16–18} The intermetallic phases in the present work were obtained by seeded growth and high-temperature annealing at 600 °C within a protective mesoporous silica (mSiO₂) shell.¹⁹ In experiments with p-H₂, the surface structure of Pt–Sn intermetallic nanoparticles (iNPs) has played a role in several extraordinary spin polarization phenomena. Pt₃Sn@mSiO₂ iNPs were shown to mediate conversion of p-H₂ singlet order into hyperpolarization of liquid water and alcohols,²⁰ and PtSn@mSiO₂ iNPs were previously shown to catalyze hydrogenation of propene (PE) to propane (PA) with a high pairwise selectivity of 10%.²¹ Remarkably, PtSn@mSiO₂ iNPs exhibited a 3000-fold higher pairwise selectivity relative to similarly sized monometallic Pt@mSiO₂ NPs. A key difference between the two is the absence of 3-fold Pt(111) hollow sites on PtSn. These sites have been implicated in the facile H₂ dissociation^{22–24} and fast H adatom diffusion on Pt(111) surfaces where such sites are contiguous.⁶²

In the literature, significant differences in conversion and pairwise selectivity have been observed in the hydrogenation of

Received: February 27, 2022

Accepted: April 15, 2022

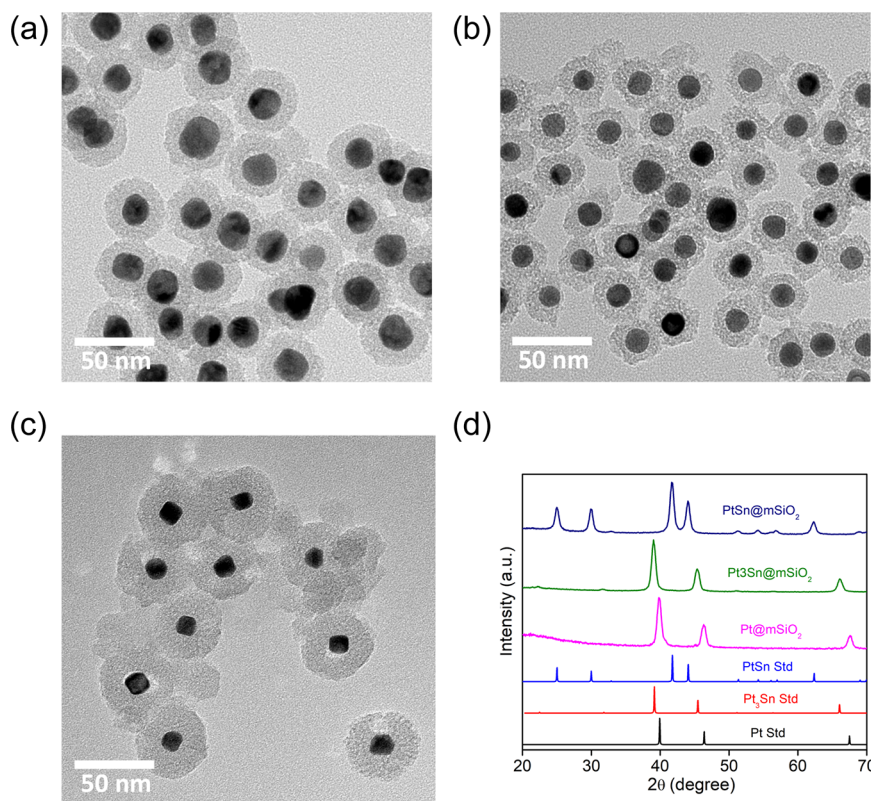


Figure 1. TEM images of (A) PtSn@mSiO_2 , (B) $\text{Pt}_3\text{Sn@mSiO}_2$, and (C) Pt@mSiO_2 NPs and (D) PXRD patterns.

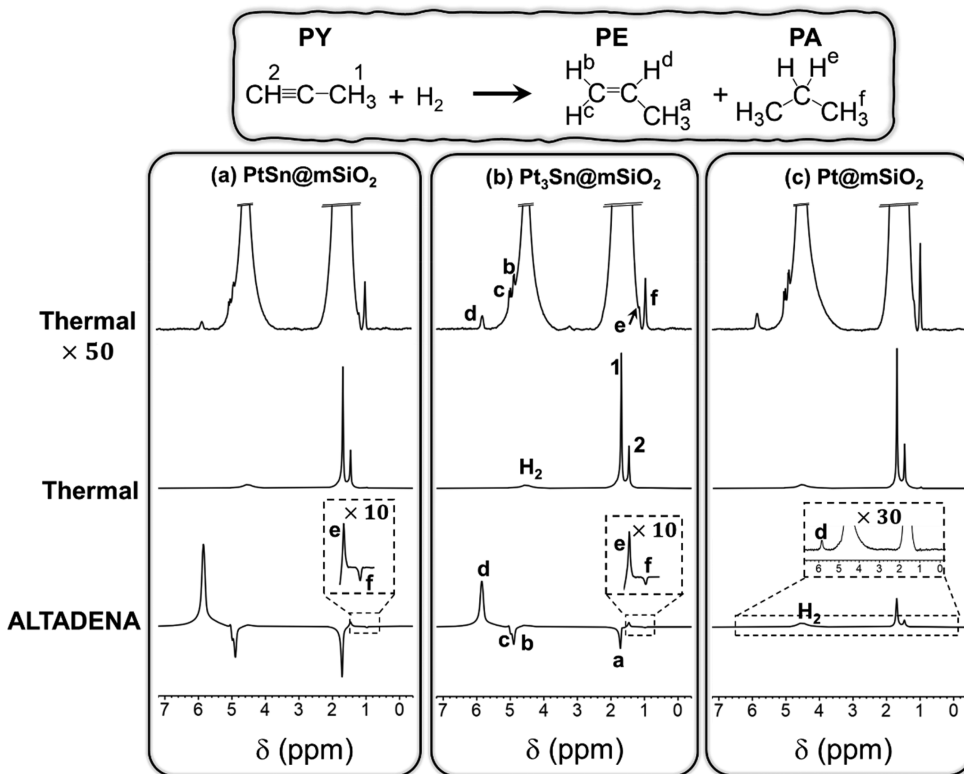


Figure 2. Thermally polarized (top: $\times 50$ and middle) and ALTADENA (bottom) ^1H NMR spectra of reaction effluent in propyne hydrogenation with 50% p- H_2 over 15 mg of (a) PtSn@mSiO_2 , (b) $\text{Pt}_3\text{Sn@mSiO}_2$, and (c) Pt@mSiO_2 at 250 $^\circ\text{C}$. The reactant gas consisted of 120/70/210 mL/min of $\text{H}_2/\text{N}_2/\text{propane}$.

alkynes vs alkenes over the same catalysts. For instance, an increase in the signal enhancement by an order of magnitude

was reported in the hydrogenation of propyne (PY) compared to hydrogenation of PE using a silica-supported vanadium oxo

organometallic catalyst.²⁵ Similar observations were reported for other catalytic systems such as immobilized iridium complexes²⁶ and silica/alumina/zirconia supported Pd NPs.²⁷ The present study of PY hydrogenation was aimed at exploring the potentially higher performance, in terms of both conversion and pairwise selectivity, that may be achieved for the alkyne hydrogenation over the Pt₃Sn and PtSn iNPs. High-resolution transmission electron microscopy (TEM) images and powder X-ray diffraction patterns (PXRD) of Pt@mSiO₂, Pt₃Sn@mSiO₂, and PtSn@mSiO₂ NPs are presented in Figure 1.

In the ALTADENA experiment,²⁸ hydrogenation with p-H₂ is performed near zero magnetic field followed by transport of the products under adiabatic passage conditions to high field for NMR detection. In our experiments, the U-tube reactor was positioned in the 5 mT fringe field of the 9.4 T Bruker Ultrashield superconducting magnet, and transport occurred via gas flow through tubing connecting the outlet of the U-tube and the detection coil of the NMR probe. Further details are provided in the *Experimental Methods* section.

Figure 2 presents the 400 MHz ¹H ALTADENA NMR spectra of the reactor effluent in the hydrogenation of PY with 50% p-H₂ at a reactor temperature of 250 °C. The corresponding spectra acquired after allowing the nuclear spins to fully relax to thermal equilibrium are also presented. The signal enhancement factor is defined as the ratio of the ALTADENA and thermal equilibrium NMR signals after each is divided by its respective number of accumulated transients. The pairwise selectivity is estimated as the ratio of the observed and theoretical enhancement factors.²⁹ The formulas are included in the *Supporting Information*. In the ALTADENA spectra, the PE –CH^d proton and one of the PE –CH₂ protons, either H^b for *syn*-addition or H^c for *anti*-addition, originate from p-H₂. Notably, the PE –CH₃ group signal (peak “a”) is very intense, with an absolute intensity similar to that of –CH^d, even though no methyl protons originated from p-H₂. This sharing of p-H₂ spin order stems from a combination of two effects: (1) mixing of the methyl proton spin states into the low field eigenstates incorporating the p-H₂ protons and (2) transfer of spin order resulting from the rapid adiabatic transport through level anticrossings induced by proton–proton spin coupling. Therefore, to calculate the pairwise selectivity from the enhancement factor for a specific proton peak, the theoretical enhancement factor for that site needs to be known. Density matrix simulations³⁰ (see the *Supporting Information*) show that the enhancement factor for the PE –CH^d proton depends on the stereochemistry of addition to PY. The ¹H signal enhancement factors for pure *syn*- or *anti*-addition of 50% p-H₂ are calculated to be 5175 and 8072, respectively, at 9.4 T and 298 K. Hence, quantitation of the stereoselectivity is necessary for the accurate estimate of the pairwise selectivity. Because *syn*- and *anti*-addition yield distinct PE ALTADENA spectral features (Figure S1), the stereoselectivity can be estimated by fitting the experimental spectrum to a linear combination of simulated *syn*- and *anti*-addition ALTADENA spectra.³¹

The spectral fitting, shown in Figure S2, indicates a stereoselectivity of 69 ± 2% *syn*-addition for PtSn@mSiO₂ at 250 °C, corresponding to a theoretical enhancement factor of 6073 ± 58 for H^d. For the same catalyst, the maximum experimentally measured signal enhancement factor was 1198 ± 67 after correction for spin–lattice relaxation losses during transport from the U-tube to the NMR probe (see the

Supporting Information for details). Hence, the pairwise selectivity is 19.7 ± 1.1% (15.8% uncorrected). This is the highest pairwise selectivity to be reported for a supported metal catalyst in a gas/solid heterogeneous reaction.

Figure 3a,b compares the observed signal enhancements for PE and PA and the corresponding pairwise selectivities for all

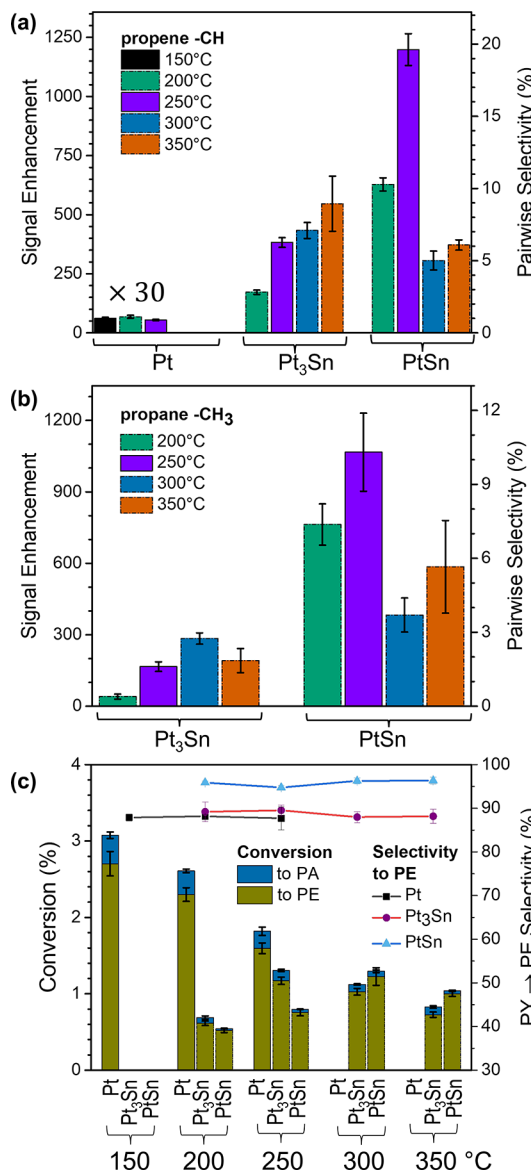


Figure 3. (a) Propene –CH peak and (b) propane –CH₃ peak signal enhancement factors and pairwise selectivity in the hydrogenation of propyne over Pt@mSiO₂, Pt₃Sn@mSiO₂, and PtSn@mSiO₂ at temperatures from 150 to 350 °C. (c) Partial hydrogenation selectivity and percent conversions to propene and propane.

three catalysts at temperatures ranging from 150 to 350 °C. Consistent with the results for PE hydrogenation,²¹ introduction of Sn to form the intermetallic phase drastically affects the signal enhancements of both PE and PA. Compared to the 1198-fold enhancement obtained for PtSn@mSiO₂ at 250 °C,¹⁴² Pt₃Sn@mSiO₂ and Pt@mSiO₂ afforded much lower PE –CH^d peak signal enhancement factors of 382, and 2, respectively, at the same temperature.¹⁴³

Hyperpolarized and thermally polarized PA peaks (“e” and “f”) were also detected with pairwise selectivities of 10.3%,¹⁴⁴

148 1.6%, and 0% for PtSn, Pt₃Sn, and Pt at 250 °C, respectively.
149 The 10.3% pairwise selectivity of PtSn@mSiO₂ is similar to the
150 value obtained in our previous study of PE hydrogenation with
151 this catalyst.²¹ The full data set with experimental uncertainties
152 for the three catalysts is provided in Figures S3 and S4 as well
153 as Tables S3–S6.

154 The percentage conversions of PY to PE and PA for the
155 three catalysts are reported in Figure 3c. For Pt@mSiO₂,
156 conversion decreased monotonically with temperature, and
157 hydrogenation products could not be detected at temperatures
158 over 300 °C. For PtSn@mSiO₂ and Pt₃Sn@mSiO₂ iNPs,
159 conversion initially increased with temperature but eventually
160 decreased slightly at higher temperatures. PY to PE conversion
161 followed the order Pt@mSiO₂ > Pt₃Sn@mSiO₂ > PtSn@mSiO₂,
162 while the pairwise selectivity exhibits the reverse trend.
163 Such an inverse relationship was reported in the hydrogenation
164 of PE to PA for this series of three catalysts.²¹ However,
165 conversion of PY was about a factor of 4 greater than the
166 conversion of PE for the same PtSn@mSiO₂ catalyst.²¹
167 Notably, the variation in conversion with the mole fraction
168 of Sn was smaller for hydrogenation of PY relative to PE. Pt@mSiO₂
169 and Pt₃Sn@mSiO₂ exhibited significantly lower
170 conversion for PY as the reactant (1–3%) compared to 15–
171 25% for PE.

172 The observed trends in conversion and signal enhancement
173 as a function of the fraction of Sn in the catalyst can be
174 rationalized based on literature studies of molecular adsorption
175 and diffusion on Pt–Sn surface alloys.

176 **Effect on Density of Adsorbed PY.** TPD measurements
177 show that the adsorption energy of PY decreases from 161 kJ/
178 mol on Pt(111) to 119 kJ/mol on p(2 × 2) Pt₃Sn(111) to 96
179 kJ/mol on ($\sqrt{3} \times \sqrt{3}$) R30° Pt₂Sn(111),¹⁰ where the surface
180 overlayer structure is specified by using Wood's notation.
181 Therefore, the density of adsorbed PY is expected to decrease
182 as the Sn fraction increases, thereby lowering conversion.
183 Pairwise selectivity for alkyne hydrogenation was about a factor
184 of 2 higher than for alkene hydrogenation. Because of the
185 much stronger adsorption of the alkyne compared to H₂, the
186 metal surface is almost completely covered by PY molecules,
187 and H₂ can only be adsorbed within the interspace between
188 them, which can be expected to further hinder H adatom
189 diffusion.

190 **Effect on H Adatom Density.** Dissociative D₂ chem-
191 isorption on Pt/Sn alloys has been studied by hyperthermal
192 molecular beam experiments. On Pt(111) surfaces, the
193 activation energy barrier of D₂ dissociation was reported to
194 be 2 kJ/mol, while a slightly higher barrier was observed on
195 p(2 × 2) Pt₃Sn(111) surface.^{24,32} On ($\sqrt{3} \times \sqrt{3}$) R30°
196 Pt₂Sn(111), the barrier increased to 27 kJ/mol. Inhibition of
197 dissociative H₂ chemisorption reduces the H adatom density,
198 contributing to the lower conversions observed on PtSn iNPs.
199 Moreover, a TPD study demonstrated that the saturation
200 coverage of D adatoms decreases from 0.95 monolayer (ML)
201 on Pt(111) to 0.68 ML on p(2 × 2) Pt₃Sn(111) and 0.51 ML
202 on ($\sqrt{3} \times \sqrt{3}$) R30° Pt₂Sn(111) at 110 K.²³ For PtSn iNPs,
203 the absence of 3-fold Pt₃ hollow sites is expected to further
204 decrease coverage and conversion.²⁴

205 **Effect on Direct Addition of Molecular H₂.** Because of
206 the high barrier to dissociate H₂ molecules on PtSn (ca. 29 kJ/
207 mol),¹⁹ the fraction of adducts formed by direct addition of
208 molecular H₂ is expected to be higher on this surface. In direct
209 addition, both H atoms in molecular H₂ approach the carbon–

210 carbon triple bond from the same side in a reaction path
211 favoring concerted, pairwise hydrogenation.²¹

Effect on the Activation Energy Barrier of H Adatom

212 **Diffusion.** The activation energy of H adatom diffusion
213 increases with increasing Sn content due to the loss of 3-fold
214 Pt₃ hollow sites where high coordination Pt₃–H binding
215 occurs.²⁴ The DFT study by Fearon and Watson indicates that
216 the maximum energy barriers of hydrogen diffusion on
217 Pt(111), p(2 × 2) Pt₃Sn(111), and ($\sqrt{3} \times \sqrt{3}$) R30°
218 Pt₂Sn(111) are 5, 41, and 100 kJ/mol, respectively (PtSn
219 (110) was not included in that study).²² By restricting
220 diffusion, the lifetime of proton singlet spin order on H
221 adatom pairs is prolonged. For the fraction of hydrogenation
222 adducts formed by stepwise addition, elevation of the barrier to
223 H adatom diffusion on Pt–Sn surfaces will have the effect of
224 increasing the pairwise selectivity. This picture is consistent
225 with an experimental para–ortho H₂ back-conversion flow
226 study,²⁰ which revealed that para–ortho back-conversion is
227 negligible below 200 °C on PtSn@mSiO₂. The decrease in
228 pairwise selectivity above 250 °C is consistent with increased
229 dissociation of H₂ on PtSn@mSiO₂ iNPs at higher temper-
230 atures.

231 As seen in Figure 3c, the partial hydrogenation selectivity
232 (PHS) to PE was >87% for all three catalysts. Similarly high
233 PHS was reported for alkyne hydrogenations on Pd
234 catalysts.^{27,33,34} The PE produced from partial hydrogenation
235 has a lower adsorption energy than that of PY, resulting in PE
236 replacement by PY in the feed.³⁴ This is also evidenced by a
237 TPD study of Pt(111), p(2 × 2) Pt₃Sn(111), and ($\sqrt{3} \times \sqrt{3}$)
238 R30° Pt₂Sn(111) showing that the adsorption energy
239 decreases from 161, 119, and 96 kJ/mol for PY to 73, 62,
240 and 49 kJ/mol for PE, respectively.^{10,13} Of the three catalysts,
241 PtSn@mSiO₂ achieved the highest PHS of 95% at all
242 temperatures, while lower PHS values were recorded for
243 Pt₃Sn and Pt NPs. The PHS of the three catalysts may also be
244 affected by differences in the H₂ dissociation. As noted above,
245 the density of H adatoms on the PtSn catalysts will be reduced
246 because of the higher barrier of H₂ dissociation, thus inhibiting
247 the over-hydrogenation to PA.

248 Activity loss was observed in experiments with all three
249 catalysts at elevated temperatures and is attributed to
250 accumulation of carbonaceous deposits.^{35,36} DFT studies
251 indicate that the onset of C–C scission on the Pt(111)
252 surface proceeds through PY due to its relatively strong
253 adsorption and large exothermicity compared to other C₃H_x (x
254 = 3–8) hydrocarbons.¹⁷ Moreover, Peck et al. reported that
255 ~80% of chemisorbed PY on Pt (111) undergoes decom-
256 position to form surface carbons by post-TPD AES experi-
257 ments.¹⁰ However, the incorporation of Sn in Pt/Sn alloys can
258 delay the progression toward deactivation. In this study, the
259 conversion of PY to PE started to decline at 150, 250, and 350
260 °C on Pt@mSiO₂, Pt₃Sn@mSiO₂, and PtSn@mSiO₂,
261 respectively (Figure 3c and Figure S5). This demonstrates
262 that the incorporation of Sn can effectively reduce but not
263 eliminate the deactivation due to coke formation.^{37,38}

264 Methods for catalyst regeneration to restore the activity of
265 spent Pt–Sn alloys have been extensively investigated.^{37,39,40}
266 A typical regeneration procedure consists of exposing used
267 catalysts to O₂ or air at high temperatures to burn off the
268 carbonaceous deposits followed by a reduction in H₂.^{39,41,42} In
269 the present work, to examine if the performance of three Pt–
270 Sn@mSiO₂ NPs is recovered after vigorous PY hydrogenation

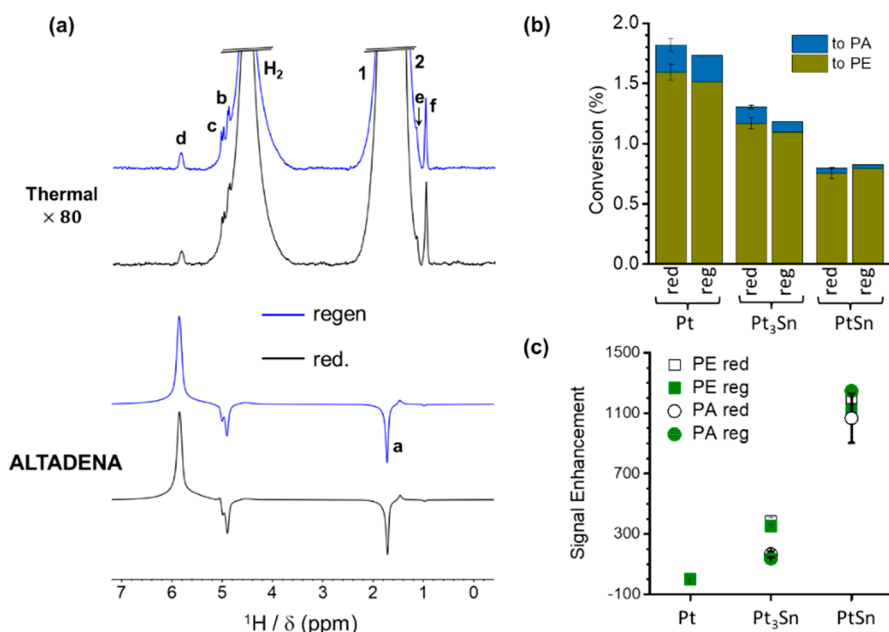


Figure 4. (a) Thermal and ALTADENA spectra acquired after initial reduction (red) and after regeneration (reg) of spent PtSn@mSiO₂ catalyst. (b) Percent conversions and (c) signal enhancement factors in the hydrogenation of propyne over Pt@mSiO₂, Pt₃Sn@mSiO₂, and PtSn@mSiO₂ at 250 °C after two catalysts treatments: (1) initial reduction in H₂ at 600 °C and (2) regeneration, consisting of oxidation in the air at 500 °C followed by a reduction in H₂ at 600 °C.

272 runs, a similar oxidation–reduction cycling regeneration
273 approach was employed. The spent Pt, Pt₃Sn, and PtSn
274 catalysts were heated under continuous air flow at 500 °C for 2
275 h followed by a reduction in H₂ at 600 °C for 2 h. As shown in
276 Figure 4, no significant difference in conversion or NMR signal
277 enhancement factor was observed for all three catalysts except
278 for a slight reduction in PE –CH signal enhancement on
279 PtSn@mSiO₂ after the regeneration as compared to the initial
280 runs (i.e., 1198 vs 1121). The measured values for the
281 conversions, signal enhancement factors, and pairwise
282 selectivities of three NPs after the oxidation–reduction cycling
283 are summarized in Figure S6 and Table S7. The restoration in
284 the performance of three NPs is likely due to the removal of
285 surface carbon deposits during the catalyst regeneration
286 process.^{43–46} Thus, Pt₃Sn@mSiO₂ and PtSn@mSiO₂ iNPs
287 are robust and effective catalysts for achieving high NMR
288 signal enhancement with excellent durability and recyclability
289 in parahydrogen enhanced NMR. For these catalysts, the
290 mSiO₂ shell effectively prevents the encapsulated iNPs from
291 aggregation at high temperatures.

292 To summarize, conversion of PY to PE followed the trend
293 Pt@mSiO₂ > Pt₃Sn@mSiO₂ > PtSn@mSiO₂ while signal
294 enhancement (and pairwise selectivity) followed the reverse
295 order. The same trends were observed for the hydrogenation
296 of PE to PA in ref 21. The PtSn@mSiO₂ iNPs exhibited a 19.7
297 ± 1.1% pairwise selectivity in the hydrogenation of PY to PE at
298 250 °C, which is the highest pairwise selectivity to be observed
299 for a supported metal nanoparticle catalyst. In contrast,
300 similarly sized Pt@mSiO₂ NPs exhibited a maximum pairwise
301 selectivity of only 0.04%. The main difference between the Pt
302 and PtSn surfaces is the occurrence of contiguous 3-fold Pt
303 sites on the former. These sites have been implicated in the
304 facile H₂ dissociation and H adatom diffusion on Pt(111)
305 surfaces. Restriction of diffusion will prolong the lifetime of
306 singlet spin order in an H adatom pair originating from a p-H₂
307 molecule. Direct addition of molecular H₂, which is inherently

pairwise, can also explain the high pairwise selectivity observed 308 for the PtSn catalyst. The hypothesis for direct molecular 309 addition is supported by the results of a para–ortho H₂ back- 310 conversion flow study in ref 20, which showed that 311 temperatures above 200 °C are necessary to activate para– 312 ortho conversion on PtSn@mSiO₂ iNPs. The decrease in 313 pairwise selectivity above 250 °C is consistent with increased 314 H₂ dissociation on PtSn@mSiO₂ iNPs at elevated temper- 315 atures. Because the observed pairwise selectivity of PY 316 hydrogenation is well below 100%, it appears that a substantial 317 fraction of adducts are formed by stepwise addition. Therefore, 318 the possibility of significant parallel contributions from both 319 paths cannot be excluded. 320

PY hydrogenation was found to occur with nearly twice the 321 pairwise selectivity as PE hydrogenation. We hypothesize that 322 this is due to the higher coverage of the former and the 323 resulting restriction of diffusion. The relatively low conversion 324 of PY hydrogenation using 15 mg of PtSn@mSiO₂ (ca. 1%) is 325 not unexpected given the high 400 mL/min flow rate used in 326 the present work, which is necessary to avoid spin relaxation 327 during transport to the NMR probe. Under these conditions, 328 even the conversion using Pt@mSiO₂ was only 2–3%. 329

Hyperpolarized gaseous alkenes produced by continuous- 330 flow hydrogenation with parahydrogen could have interesting 331 prospective applications. For example, they could be employed 332 as hyperpolarized reactants for sensitivity enhanced NMR 333 studies of downstream catalytic transformations, not limited to 334 hydrogenation. Another possibility is to use the hyperpolarized 335 alkenes in sensitivity enhanced operando NMR spectroscopy 336 of alkene adsorption, surface interactions, and chemical 337 transformations. Spin order transfer of proton hyperpolariza- 338 tion on the adsorbed alkene to other chemical species, 339 including nuclear spins at active sites of catalysts, could 340 widen the scope of such an approach. 341

Finally, we demonstrated that the activity of the silica 342 encapsulated catalysts, which is diminished at higher temper- 343

344 atures due to the formation of carbonaceous deposits, can be
345 readily recovered by the oxidation–reduction cycling, which
346 proves that the activity loss is not due to surface reconstruction
347 or phase separation. With the advantages of high activity,
348 selectivity, stability, and the ease of separation from the
349 hydrogenation products, the Pt–Sn@mSiO₂ iNPs materials
350 provide an attractive catalytic platform for producing hyper-
351 polarized gases and liquids.

352 ■ EXPERIMENTAL METHODS

353 **Platinum and Platinum–Tin Nanoparticles.** Details of
354 the syntheses of Pt@mSiO₂ and Pt–Sn@mSiO₂ NPs have
355 been published previously⁸ and are also included in the
356 **Supporting Information.** Briefly, the core–shell structured Pt@
357 mSiO₂ NPs were synthesized by using tetradecyltrimethyl-
358 ammonium bromide-capped (TTAB-capped) Pt NPs as initial
359 core material for the subsequent silica polymerization with
360 tetraethyl orthosilicate (TEOS), followed by removal of TTAB
361 molecules in the calcination. The intermetallic phases of PtSn
362 and Pt₃Sn were prepared by heterogeneous nucleation of Sn
363 from SnCl₂·2H₂O at the metal surface of Pt@mSiO₂ in
364 tetraethylene glycol. The metal loadings, particle sizes, Pt
365 dispersion, and the surface site densities of three NPs are
366 summarized in Table S1. Additional characterizations of the
367 three catalysts are presented in the **Supporting Information**
368 and in previous publications.^{8,21}

369 **Hydrogenation.** Hydrogen enriched to 50% p-H₂ was
370 prepared by flowing normal ultrahigh purity H₂ gas through a
371 liquid nitrogen cooled coiled copper tube (0.25 in. O.D.)
372 containing iron oxide hydroxide, as described elsewhere.⁴⁷
373 Hydrogenation of gaseous PY was performed under
374 ALTADENA²⁸ conditions where the reaction is performed in
375 the fringe field of the 9.4 T Bruker Avance Ultrashield
376 superconducting magnet, and the reactor effluent containing
377 products and unreacted reactants is transported by flow to a
378 standard Bruker 10 mm liquids probe for NMR detection at
379 400 MHz. The reaction mixture containing H₂ and PY as
380 reactants and N₂ as a dilutant buffer gas was premixed by
381 combining the outputs of three mass flow controllers (Alicat
382 Scientific) set to flow rates of 120/210/70 mL/min. The
383 mixture was fed into a U-shaped quartz tube (0.25 in. O.D.;
384 0.15 in. I.D.) reactor packed with 15 mg of Pt@mSiO₂,
385 Pt₃Sn@mSiO₂, or PtSn@mSiO₂ catalysts. The catalyst was
386 held in place with quartz wool. The temperature in the reactor
387 U-tube was regulated by a home-built temperature controller
388 with feedback from a K-type thermocouple inserted directly
389 into the catalyst bed. The gaseous reactor effluent flowed
390 through PFA tubing (0.125 in. O.D.; 0.0625 in. I.D.; 1 m
391 length) and was delivered through a thin glass capillary to the
392 bottom of a 10 mm O.D. NMR tube inserted into the NMR
393 probe. ALTADENA mode NMR spectra were collected by
394 accumulating 64 free induction decays with a 2 s recycle delay
395 with gases flowing continuously. For each catalyst, the
396 hydrogenation reaction was repeated by using n-H₂. Thermally
397 polarized spectra at Boltzmann equilibrium were acquired by
398 accumulating 512 free induction decays with a recycle delay of
399 6 s under the nonflowing condition with the gas effluent sealed
400 in the NMR sample loop. The spectra were processed by using
401 MestReNova ver. 14.2 software, and the signal integrals of the
402 propene –CH, propane –CH₃, and propyne –CH peaks of the
403 the ALTADENA and thermally polarized NMR spectra were
404 obtained by multiplet fitting. The peak height, line width, and

405 Lorentzian/Gaussian ratio were varied to optimize the fit while
406 the chemical shifts were fixed.²⁵

407 **Catalyst Treatments.** Two different catalyst activation
408 treatments were employed in the present work. Freshly
409 synthesized Pt₃Sn and PtSn catalysts were reduced at 600 °C
410 and Pt catalysts at 300 °C in a stream of 90/10 mL/min of N₂/
411 H₂ for 2 h before performing hydrogenation reactions.
412 Regeneration treatments on spent catalysts consisted of
413 oxidation–reduction cycling and were performed after catalyst
414 deactivation at higher reaction temperatures. To restore the
415 activity of the Pt–Sn@mSiO₂ iNPs, the catalyst was oxidized
416 with 50 mL/min of air at 500 °C for 2 h, followed by the
417 reduction with 90/10 mL/min of N₂/H₂ at 600 °C for 2 h. In
418 both catalyst treatments, the hydrogenation reactor was cooled
419 to room temperature prior to starting the hydrogenation
420 reactions.

421 ■ ASSOCIATED CONTENT

422 ■ Supporting Information

423 The Supporting Information is available free of charge at
424 <https://pubs.acs.org/doi/10.1021/acs.jpcllett.2c00581>.

425 Information about the catalyst synthesis and character-
426 ization, catalyst turnover frequencies, numerical density
427 matrix simulations details, formulas used for calculation
428 of the conversion, pairwise selectivity, spectral fitting,
429 and NMR signal enhancement, as well as tabulated
430 numerical values for these values at all temperature
431 studied; the complete set of all ALTADENA and
432 thermal equilibrium experimental spectra that were
433 acquired in this study (PDF)

434 ■ AUTHOR INFORMATION

435 Corresponding Authors

436 Clifford R. Bowers – Department of Chemistry and National
437 High Magnetic Field Laboratory, University of Florida,
438 Gainesville, Florida 32611, United States;  orcid.org/0000-0001-6155-5163; Email: bowers@chem.ufl.edu

439 Wenyu Huang – Department of Chemistry, Iowa State
440 University, Ames, Iowa 50011, United States; Ames
441 Laboratory, U.S. Department of Energy, Ames, Iowa 50011,
442 United States;  orcid.org/0000-0003-2327-7259;
443 Email: whuang@iastate.edu

444 Authors

445 Yong Du – Department of Chemistry and National High
446 Magnetic Field Laboratory, University of Florida, Gainesville,
447 Florida 32611, United States

448 Ranjan K. Behera – Department of Chemistry, Iowa State
449 University, Ames, Iowa 50011, United States

450 Raghu V. Maligal-Ganesh – Department of Chemistry, Iowa
451 State University, Ames, Iowa 50011, United States;
452  orcid.org/0000-0001-8332-4454

453 Minda Chen – Department of Chemistry, Iowa State
454 University, Ames, Iowa 50011, United States;  orcid.org/0000-0002-9881-9350

455 Tommy Yunpu Zhao – Department of Chemistry and
456 National High Magnetic Field Laboratory, University of
457 Florida, Gainesville, Florida 32611, United States

458 Complete contact information is available at:
459 <https://pubs.acs.org/doi/10.1021/acs.jpcllett.2c00581>

462 Notes

463 The authors declare no competing financial interest.

464 ■ ACKNOWLEDGMENTS

465 This work was supported by NSF Grants CHE-1808239 and
466 CHE-2108306/2108307 (C.R.B. and W.H.) and the National
467 High Magnetic Field Laboratory's User Collaborative Grant
468 Program, supported by the National Science Foundation
469 Cooperative Agreement DMR-1644779* and the State of
470 Florida.

471 ■ REFERENCES

472 (1) Bowers, C. R.; Weitekamp, D. P. Parahydrogen and Synthesis
473 Allow Dramatically Enhanced Nuclear Alignment. *J. Am. Chem. Soc.*
474 **1987**, *109* (18), 5541–5542.

475 (2) Bowers, C. R.; Weitekamp, D. P. Transformation of
476 Symmetrization Order to Nuclear-Spin Magnetization by Chemical
477 Reaction and Nuclear Magnetic Resonance. *Phys. Rev. Lett.* **1986**, *57*
478 (21), 2645–2648.

479 (3) Schmidt, A. B.; Hövener, J. B.; Bowers, C. R.; Buckenmaier, K.;
480 Chekmenev, E. Y.; de Maissin, H.; Eills, J.; Ellermann, F.; Glöggler, S.;
481 Gordon, J. W.; Knecht, S.; Koptyug, I. v.; Kuhn, J.; Pravdivtsev, A. N.;
482 Reineri, F.; Theis, T.; Them, K. Instrumentation for Hydrogenative
483 Parahydrogen-Based Hyperpolarization Techniques. *Anal. Chem.*
484 **2022**, *94* (1), 479–502.

485 (4) Pokochueva, E.; Burueva, D.; Kovtunova, L.; Bukhtiyarov, A.;
486 Gladky, A.; Kovtunov, K. v.; Koptyug, I. v.; Bukhtiyarov, V.
487 Mechanistic In Situ Investigation of Heterogeneous Hydrogenation
488 over Rh/TiO₂ Catalysts: Selectivity, Pairwise Route, Catalyst Nature.
489 *Faraday Discuss.* **2021**, *229*, 161.

490 (5) Song, B.; Choi, D.; Xin, Y.; Bowers, C. R.; Hagelin-Weaver, H.
491 Ultra-Low Loading Pt/CeO₂ Catalysts: Ceria Facet Effect Affords
492 Improved Pairwise Selectivity for Parahydrogen Enhanced NMR
493 Spectroscopy. *Angew. Chem., Int. Ed.* **2021**, *60* (8), 4038–4042.

494 (6) Panja, C.; Saliba, N. A.; Koel, B. E. Coking Resistance of Pt–Sn
495 Alloys Probed by Acetylene Chemisorption. *Catal. Lett.* **2000**, *68* (3),
496 175–180.

497 (7) Panja, C.; Saliba, N. A.; Koel, B. E. Acetylene Chemisorption on
498 Sn/Pt(100) Alloys. *J. Phys. Chem. B* **2001**, *105* (18), 3786–3796.

499 (8) Maligal-Ganesh, R. V.; Xiao, C.; Goh, T. W.; Wang, L.-L.;
500 Gustafson, J.; Pei, Y.; Qi, Z.; Johnson, D. D.; Zhang, S.; Tao, F.;
501 Huang, W. A Ship-in-a-Bottle Strategy To Synthesize Encapsulated
502 Intermetallic Nanoparticle Catalysts: Exemplified for Furfural Hydro-
503 genation. *ACS Catal.* **2016**, *6* (3), 1754–1763.

504 (9) Bariås, O. A.; Holmen, A.; Blekkan, E. A. Propane Dehydrogen-
505 ation over Supported Pt and Pt–Sn Catalysts: Catalyst Preparation,
506 Characterization, and Activity Measurements. *J. Catal.* **1996**, *158* (1),
507 1–12.

508 (10) Peck, J. W.; Mahon, D. I.; Koel, B. E. A Temperature
509 Programmed Desorption Study of the Reaction of Methylacetylene on
510 Pt(111) and Sn/Pt(111) Surface Alloys. *Surf. Sci.* **1998**, *410* (2),
511 200–213.

512 (11) Tsai, Y.-L.; Koel, B. E. Temperature-Programmed Desorption
513 Investigation of the Adsorption and Reaction of Butene Isomers on
514 Pt(111) and Ordered Pt–Sn Surface Alloys. *J. Phys. Chem. B* **1997**,
515 *101* (15), 2895–2906.

516 (12) Zhao, H.; Koel, B. E. Influence of Coadsorbed Hydrogen on
517 Ethylene Adsorption and Reaction on a $(\sqrt{3}\times\sqrt{3})R30^\circ$ -Sn/Pt(111)
518 Surface Alloy. *Langmuir* **2005**, *21* (3), 971–975.

519 (13) Tsai, Y.-L.; Xu, C.; Koel, B. E. Chemisorption of Ethylene,
520 Propylene and Isobutylene on Ordered Sn/Pt(111) Surface Alloys.
521 *Surf. Sci.* **1997**, *385* (1), 37–59.

522 (14) Zhao, H.; Koel, B. E. Reactivity of Ethyl Groups on a Sn/
523 Pt(111) Surface Alloy. *Catal. Lett.* **2005**, *99* (1), 27–32.

524 (15) Batzill, M.; Beck, D. E.; Koel, B. E. Electronic Contrast in
525 Scanning Tunneling Microscopy of Sn–Pt(111) Surface Alloys. *Surf.*
526 *Sci.* **2000**, *466* (1), L821–L826.

527 (16) Yang, M.-L.; Zhu, Y.-A.; Zhou, X.-G.; Sui, Z.-J.; Chen, D. First-
528 Principles Calculations of Propane Dehydrogenation over PtSn
529 Catalysts. *ACS Catal.* **2012**, *2* (6), 1247–1258.

530 (17) Yang, M. L.; Zhu, Y. A.; Fan, C.; Sui, Z. J.; Chen, D.; Zhou, X.
531 G. Density Functional Study of the Chemisorption of C1, C2 and C3
532 Intermediates in Propane Dissociation on Pt(1 1 1). *J. Mol. Catal. A: Chem.* **2010**, *321*, 42.

533 (18) Nykänen, L.; Honkala, K. Density Functional Theory Study on
534 Propane and Propene Adsorption on Pt(111) and PtSn Alloy
535 Surfaces. *J. Phys. Chem. C* **2011**, *115* (19), 9578–9586.

536 (19) Pei, Y.; Maligal-Ganesh, R. v.; Xiao, C.; Goh, T.-W.; Brashler,
537 K.; Gustafson, J. A.; Huang, W. An Inorganic Capping Strategy for the
538 Seeded Growth of Versatile Bimetallic Nanostructures. *Nanoscale*
539 **2015**, *7* (40), 16721–16728.

540 (20) Zhao, E. W.; Maligal-Ganesh, R.; Du, Y.; Zhao, T. Y.; Collins,
541 J.; Ma, T.; Zhou, L.; Goh, T. W.; Huang, W.; Bowers, C. R. Surface-
542 Mediated Hyperpolarization of Liquid Water from Parahydrogen.
543 *Chem.* **2018**, *4* (6), 1387–1403.

544 (21) Zhao, E. W.; Maligal-Ganesh, R.; Xiao, C.; Goh, T.-W. W.; Qi,
545 Z.; Pei, Y.; Hagelin-Weaver, H. E.; Huang, W.; Bowers, C. R. Silica-
546 Encapsulated Pt-Sn Intermetallic Nanoparticles: A Robust Catalytic
547 Platform for Parahydrogen-Induced Polarization of Gases and
548 Liquids. *Angew. Chem.* **2017**, *129* (14), 3983–3987.

549 (22) Fearon, J.; Watson, G. W. Hydrogen Adsorption and Diffusion
550 on Pt {111} and PtSn {111}. *J. Mater. Chem.* **2006**, *16* (20), 1989–
551 1996.

552 (23) Voss, M. R.; Busse, H.; Koel, B. E. Adsorption of Thermal D
553 Atoms on Sn/Pt(111) Surface Alloys. *Surf. Sci.* **1998**, *414* (3), 330–
554 340.

555 (24) Samson, P.; Nesbitt, A.; Koel, B. E.; Hodgson, A. Deuterium
556 Dissociation on Ordered Sn/Pt(111) Surface Alloys. *J. Chem. Phys.*
557 **1998**, *109* (8), 3255–3264.

558 (25) Zhivonitko, V. v.; Skovpin, I. v.; Szeto, K. C.; Taoufik, M.;
559 Koptyug, I. v. Parahydrogen-Induced Polarization Study of the Silica-
560 Supported Vanadium Oxo Organometallic Catalyst. *J. Phys. Chem. C*
561 **2018**, *122* (9), 4891–4900.

562 (26) Skovpin, I. v.; Zhivonitko, V. V.; Kaptein, R.; Koptyug, I. V.
563 Generating Parahydrogen-Induced Polarization Using Immobilized
564 Iridium Complexes in the Gas-Phase Hydrogenation of Carbon-
565 Carbon Double and Triple Bonds. *Appl. Magn. Reson.* **2013**, *44* (1–
566 2), 289–300.

567 (27) Kovtunov, K. v.; Beck, I. E.; Zhivonitko, V. v.; Barskiy, D. A.;
568 Bukhtiyarov, V. I.; Koptyug, I. v. Heterogeneous Addition of H2 to
569 Double and Triple Bonds over Supported Pd Catalysts: A
570 Parahydrogen-Induced Polarization Technique Study. *Phys. Chem.*
571 *Chem. Phys.* **2012**, *14* (31), 11008–11014.

572 (28) Pravica, M. G.; Weitekamp, D. P. Net NMR Alignment by
573 Adiabatic Transport of Parahydrogen Addition Products to High
574 Magnetic Field. *Chem. Phys. Lett.* **1988**, *145* (4), 255–258.

575 (29) Kovtunov, K. v.; Salnikov, O. G.; Zhivonitko, V. v.; Skovpin, I.
576 v.; Bukhtiyarov, V. I.; Koptyug, I. v. Catalysis and Nuclear Magnetic
577 Resonance Signal Enhancement with Parahydrogen. *Top. Catal.* **2016**,
578 *59* (19), 1686–1699.

579 (30) Bengs, C.; Levitt, M. H. SpinDynamica: Symbolic and
580 Numerical Magnetic Resonance in a Mathematica Environment.
581 *Magn. Reson. Chem.* **2018**, *56* (6), 374–414.

582 (31) Zhou, R.; Cheng, W.; Neal, L. M.; Zhao, E. W.; Ludden, K.;
583 Hagelin-Weaver, H. E.; Bowers, C. R. Parahydrogen Enhanced NMR
584 Reveals Correlations in Selective Hydrogenation of Triple Bonds over
585 Supported Pt Catalyst. *Phys. Chem. Chem. Phys.* **2015**, *17* (39),
586 26121–26129.

587 (32) Busse, H.; Voss, M. R.; Jerdev, D.; Koel, B. E.; Paffett, M. T.
588 Adsorption and Reaction of Gaseous H(D) Atoms with D(H)
589 Adatoms on Pt(111) and Sn/Pt(111) Surface Alloys. *Surf. Sci.* **2001**,
590 *490* (1), 133–143.

591 (33) Bond, G. C.; Webb, G.; Wells, P. B.; Winterbottom, J. M.
592 Patterns of Behavior in Catalysis by Metals. *J. Catal.* **1962**, *1* (1), 74–
593 84.

595 (34) Teschner, D.; Borsodi, J.; Wootsch, A.; Révay, Z.; Hävecker,
596 M.; Knop-Gericke, A.; Jackson, S. D.; Schlägl, R. The Roles of
597 Subsurface Carbon and Hydrogen in Palladium-Catalyzed Alkyne
598 Hydrogenation. *Science* (1979) **2008**, 320 (5872), 86–89.

599 (35) Kennedy, D. R.; Webb, G.; Jackson, S. D.; Lennon, D. Propyne
600 Hydrogenation over Alumina-Supported Palladium and Platinum
601 Catalysts. *Applied Catalysis A: General* **2004**, 259 (1), 109–120.

602 (36) Kennedy, D. R.; Cullen, B.; Lennon, D.; Webb, G.; Dennison,
603 P. R.; Jackson, S. D. Propyne Hydrogenation over a Silica-Supported
604 Platinum Catalyst Studied under Transient Conditions. *Stud. Surf. Sci.*
605 *Catal.* **1999**, 122, 125–132.

606 (37) Sun, C.; Luo, J.; Cao, M.; Zheng, P.; Li, G.; Bu, J.; Cao, Z.;
607 Chen, S.; Xie, X. A Comparative Study on Different Regeneration
608 Processes of Pt-Sn/ Γ -Al₂O₃ Catalysts for Propane Dehydrogenation.
609 *Journal of Energy Chemistry* **2018** **2018**, 27 (1), 311–318.

610 (38) Pham, H. N.; Sattler, J. J. H. B.; Weckhuysen, B. M.; Datye, A.
611 K. Role of Sn in the Regeneration of Pt/ γ -Al₂O₃ Light Alkane
612 Dehydrogenation Catalysts. *ACS Catal.* **2016**, 6 (4), 2257–2264.

613 (39) Deng, L.; Zhou, Z.; Shishido, T. Behavior of Active Species on
614 Pt-Sn/SiO₂ Catalyst during the Dehydrogenation of Propane and
615 Regeneration. *Applied Catalysis A: General* **2020**, 606, 117826.

616 (40) Afonso, J. C.; Aranda, D. A. G.; Schmal, M.; Frety, R.
617 Regeneration of a Pt-Sn/Al₂O₃ Catalyst: Influence of Heating Rate,
618 Temperature and Time of Regeneration. *Fuel Process. Technol.* **1997**,
619 50 (1), 35–48.

620 (41) Afonso, J. C.; Aranda, D. A. G.; Schmal, M.; Frety, R.
621 Importance of Pretreatment on Regeneration of a Pt-Sn/Al₂O₃
622 Catalyst. *Fuel Process. Technol.* **1995**, 42 (1), 3–17.

623 (42) Iglesias-Juez, A.; Beale, A. M.; Maaijen, K.; Weng, T. C.;
624 Glatzel, P.; Weckhuysen, B. M. A Combined in Situ Time-Resolved
625 UV-Vis, Raman and High-Energy Resolution X-Ray Absorption
626 Spectroscopy Study on the Deactivation Behavior of Pt and PtSn
627 Propane Dehydrogenation Catalysts under Industrial Reaction
628 Conditions. *J. Catal.* **2010**, 276 (2), 268–279.

629 (43) Argyle, M. D.; Bartholomew, C. H. Heterogeneous Catalyst
630 Deactivation and Regeneration: A Review. *Catalysts. MDPI AG*
631 February **2015**, 26, 145–269.

632 (44) Choi, Y. S.; Oh, K.; Jung, K.-D.; Kim, W.-I.; Koh, H. L.
633 Regeneration of Pt-Sn/Al₂O₃ Catalyst for Hydrogen Production
634 through Propane Dehydrogenation Using Hydrochloric Acid.
635 *Catalysts* **2020**, 10 (8), 898.

636 (45) Bond, G. C. *Metal-Catalysed Reactions of Hydrocarbons*;
637 Springer: 2005.

638 (46) Jin, Y.; Datye, A. K.; Rightor, E.; Gulotty, R.; Waterman, W.;
639 Smith, M.; Holbrook, M.; Maj, J.; Blackson, J. The Influence of
640 Catalyst Restructuring on the Selective Hydrogenation of Acetylene
641 to Ethylene. *J. Catal.* **2001**, 203 (2), 292–306.

642 (47) Zhou, R.; Zhao, E. W.; Cheng, W.; Neal, L. M.; Zheng, H.;
643 Quinones, R. E.; Hagelin-Weaver, H. E.; Bowers, C. R. Parahydrogen-
644 Induced Polarization by Pairwise Replacement Catalysis on Pt and Ir
645 Nanoparticles. *J. Am. Chem. Soc.* **2015**, 137 (5), 1938–1946.